

Short-wavelength infrared InAs/GaSb superlattice hole avalanche photodiode

Jia-Feng Liu(刘家丰), Ning-Tao Zhang(张宁涛), Yan Teng, Xiu-Jun Hao(郝修军), Yu Zhao(赵宇), Ying Chen(陈影), He Zhu(朱赫), Hong Zhu(朱虹), Qi-Hua Wu(吴启花), Xin Li(李欣), Bai-Le Chen(陈佰乐), Yong Huang(黄勇)

Citation: Chin. Phys. B . 2020, 29(11): 117301 . **doi:** 10.1088/1674-1056/aba2e0
Journal homepage: http://cpb.iphy.ac.cn; http://iopscience.iop.org/cpb

What follows is a list of articles you may be interested in

Interface and border trapping effects in normally-off Al_2O_3/AlGaN/GaN MOS-HEMTs with different post-etch surface treatments

Si-Qi Jing(荆思淇), Xiao-Hua Ma(马晓华), Jie-Jie Zhu(祝杰杰), Xin-Chuang Zhang(张新创), Si-Yu Liu(刘思雨), Qing Zhu(朱青), Yue Hao(郝跃)

Chin. Phys. B . 2020, 29(10): 107302 . **doi:** 10.1088/1674-1056/ab99bb

Trap analysis of composite 2D-3D channel in AlGaN/GaN/graded-AlGaN: Si/GaN: C multi-heterostructure at different temperatures

Sheng Hu(胡晟), Ling Yang(杨凌), Min-Han Mi(宓珉瀚), Bin Hou(侯斌), Sheng Liu(刘晟), Meng Zhang(张濛), Mei Wu(武玫), Qing Zhu(朱青), Sheng Wu(武盛), Yang Lu(卢阳), Jie-Jie Zhu(祝杰杰), Xiao-Wei Zhou(周小伟), Ling Lv(吕玲), Xiao-Hua Ma(马晓华), Yue Hao(郝跃)

Chin. Phys. B . 2020, 29(8): 087305 . **doi:** 10.1088/1674-1056/ab96a4

Effect of AlGaN interlayer on luminous efficiency and reliability of GaN-based green LEDs on silicon substrate

Jiao-Xin Guo(郭娇欣), Jie Ding(丁杰), Chun-Lan Mo(莫春兰), Chang-Da Zheng(郑畅达), Shuan Pan(潘拴), Feng-Yi Jiang(江风益)

Chin. Phys. B . 2020, 29(4): 047303 . **doi:** 10.1088/1674-1056/ab7903

Hydrodynamic simulation of chaotic dynamics in InGaAs oscillator in terahertz region

Wei Feng(冯伟)

Chin. Phys. B . 2020, 29(4): 047302 . **doi:** 10.1088/1674-1056/ab696f

Etching mask optimization of InAs/GaSb superlattice mid-wavelength infared 640×512 focal plane array

Hong-Yue Hao(郝宏玥), Wei Xiang(向伟), Guo-Wei Wang(王国伟), Ying-Qiang Xu(徐应强), Xi Han(韩玺), Yao-Yao Sun(孙瑶耀), Dong-Wei Jiang(蒋洞微), Yu Zhang(张宇), Yong-Ping Liao(廖永平), Si-Hang Wei(魏思航), Zhi-Chuan Niu(牛智川)

Chin. Phys. B . 2017, 26(4): 047303 . **doi:** 10.1088/1674-1056/26/4/047303

Short-wavelength infrared InAs/GaSb superlattice hole avalanche photodiode*

Jia-Feng Liu(刘家丰)[1,2,†], Ning-Tao Zhang(张宁涛)[4,†], Yan Teng(滕奘)[1,2], Xiu-Jun Hao(郝修军)[2,3], Yu Zhao(赵宇)[2], Ying Chen(陈影)[1,2], He Zhu(朱赫)[1,2], Hong Zhu(朱虹)[1,2], Qi-Hua Wu(吴启花)[2], Xin Li(李欣)[2], Bai-Le Chen(陈佰乐)[4,§], and Yong Huang(黄勇)[1,2,‡]

[1] *School of Nano-Tech and Nano-Bionics, University of Science and Technology of China, Hefei* 230026, *China*
[2] *Key Laboratory of Nanodevices and Applications, Suzhou Institute of Nano-Tech and Nano-Bionics, Chinese Academy of Sciences, Suzhou* 215123, *China*
[3] *School of Physical Science and Technology, ShanghaiTech University, Shanghai* 201210, *China*
[4] *School of Information Science and Technology, ShanghaiTech University, Shanghai* 201210, *China*

(Received 13 May 2020; revised manuscript received 19 June 2020; accepted manuscript online 6 July 2020)

We demonstrate two short-wavelength infrared avalanche photodiodes based on InAs/GaSb superlattice grown by metal-organic chemical vapor deposition. The difference between the two devices, namely, $p^+n^-n^+$ and $p^+nn^-n^+$, is that the $p^+nn^-n^+$ device possesses an additional middle-doped layer to separate the multiplication region from the absorption region. By properly controlling the electric field distribution in the $p^+nn^-n^+$ device, an electric field of 906 kV/cm has been achieved, which is 2.6 times higher than that in the $p^+n^-n^+$ device. At a reverse bias of −0.1 V at 77 K, both devices show a 100% cut-off wavelength of 2.25 μm. The $p^+n^-n^+$ and $p^+nn^-n^+$ show a dark current density of 1.5×10^{-7} A/cm^2 and 1.8×10^{-8} A/cm^2, and a peak responsivity about 0.35 A/W and 0.40 A/W at 1.5 μm, respectively. A maximum multiplication gain of 55 is achieved in the $p^+nn^-n^+$ device while the value is only less than 2 in the $p^+n^-n^+$ device. Exponential nature of the gain characteristic as a function of reverse bias confirms a single carrier hole dominated impact ionization.

Keywords: short-wavelength infrared, InAs/GaSb superlattice, avalanche photodiodes, metal-organic chemical vapor deposition

PACS: 73.61.Ey, 81.15.Gh, 85.30.De, 95.85.Jq **DOI:** 10.1088/1674-1056/aba2e0

1. Introduction

Infrared avalanche photodiodes (APDs) have been widely used in long range military and astronomical applications. It owns a unique virtue of amplification of weak signals without increasing the complexity of detector circuitry. Traditionally, mercury cadmium telluride (HgCdTe) has been adopted as the material for infrared APD applications. However, with the continuous improvement of device performances, InAs/GaSb strain layer superlattices (SLs) have drawn lots of attention due to the advantages of high material uniformity,[1] comparable absorption coefficient,[2] and large effective masses,[3] compared with HgCdTe detectors. In addition, with InAs/GaSb SLs detectors we are able to not only tune the bandgap to a desired infrared wavelength but also tailor the band structure to achieve electron-dominated APDs (e-APDs) or hole-dominated APDs (h-APDs).[4] Until now, both e-APDs and h-APDs based on InAs/GaSb SLs have been reported.[5,6] These devices are all mid-wavelength infrared (MWIR) APDs with homojunction pin structures grown by molecular beam epitaxy (MBE). Although attractive gain characteristics have been obtained in these devices, high dark current at large bias is still the major limiting factor for further performance improvement. In order to achieve sufficient impact ionization and optimal multiplication, it is necessary to create high electric fields. However, in a pin device, a high electric field can also lead to a high dark current. This dilemma becomes more severe in narrower bandgap materials. Therefore, to control the electric field across the device structure is of critical importance in APD devices. In this work, we evaluate the InAs/GaSb SLs short-wavelength infrared (SWIR) APDs grown by metal-organic chemical vapor deposition (MOCVD). The electrical field is manipulated by separating the multiplication region and absorption region. This is the first report, to the best of our knowledge, on the design, growth, and fabrication of InAs/GaSb SLs SWIR APDs by MOCVD.

2. Design and experiments

Two device structures, namely, $p^+n^-n^+$ and $p^+nn^-n^+$, were designed to have hole dominated avalanche photodiodes (h-APDs), as shown in Figs. 1(a) and 1(b). In Fig. 1(a), the

*Project supported by the National Natural Science Foundation of China (Grant Nos. 61874179, 61804161, and 61975121) and the National Key Research and Development Program of China (Grant No. 2019YFB2203400).

†These authors contributed equally to this work.

‡Corresponding author. E-mail: yhuang2014@sinano.ac.cn
§Corresponding author. E-mail: chenbl@shanghaitech.edu.cn

© 2020 Chinese Physical Society and IOP Publishing Ltd

$p^+n^-n^+$ device was a baseline structure consisting of a 20 nm thick p-type GaSb cap doped with Zn ($p = 2.0 \times 10^{18}$ cm^{-3}), a 200 nm thick p-type SWIR SL (p^+-SWSL) contact doped with Zn ($p = 1.0 \times 10^{18}$ cm^{-3}), a 1.5 μm thick lightly n-type SWIR SL (n^--SWSL) absorber doped with Si ($n = 2.0 \times 10^{16}$ cm^{-3}), and a 200 nm thick n-type SWIR SL (n^+-SWSL) contact doped with Si ($n = 1.0 \times 10^{18}$ cm^{-3}) from top to bottom. Compared with the $p^+n^-n^+$ device, in the $p^+nn^-n^+$ structure, an additional 200 nm thick n-type SWIR SL (n-SWSL) multiplication layer doped with Si ($n = 5.0 \times 10^{17}$ cm^{-3}) was inserted between p^+-SWSL and n^--SWSL, as shown in Fig. 1(b). For the two devices, the $p^+n^-n^+$ device adopted a conventional pin structure without electric field control, while the $p^+nn^-n^+$ device was developed with an elaborate electrical field design. Figure 1(c) shows the electrical field distribution simulation of both devices using Silvaco Atlas program. Compared to the $p^+n^-n^+$ device, the $p^+nn^-n^+$ device was designed in a way that the n-SWSL multiplication layer was completely depleted at -10 V and the electric field was completely confined in the n-SWSL multiplication layer.[7,8] In this case, generation-recombination (G-R) current can be definitely suppressed due to a thinner depletion region,[9,10] but tunneling current may increase at the same time. More importantly, the peak electric field in the $p^+nn^-n^+$ device was as high as 906 kV/cm, which will facilitate hole initiated avalanching in the $p^+nn^-n^+$ device, while in the $p^+n^-n^+$ device it was only 347 kV/cm.

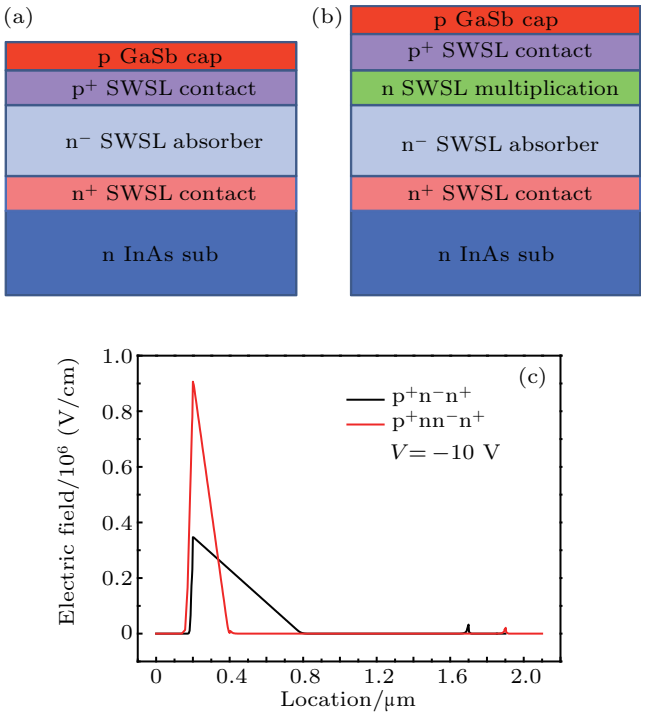


Fig. 1. The schematic cross-section of (a) $p^+n^-n^+$ device and (b) $p^+nn^-n^+$ device. (c) Simulation of electric field distribution and intensity of corresponding two devices.

The two devices were grown by MOCVD on InAs (001) substrate at 530 ℃. Details of the growth conditions can be found elsewhere.[11] The SWSL was comprised of 2 monolayer InAs/8 monolayer GaSb (2 ML/8 ML) in the two devices designed for a cut-off wavelength around 2.3 μm.[12] For device fabrication, mesas were defined using standard photolithography and chlorine-based inductively coupled plasma (ICP) dry etching. SiO_2 grown by plasma enhanced chemical vapor deposition (PECVD) was used as the passivation layer. Ti/Pt/Au metal stacks were deposited as the top and bottom contacts. The junction area of the devices had a diameter of 300 μm.

The fabricated devices were characterized in a temperature and ambient controlled probe station. Current–voltage characteristics were measured by Agilent B1500 A precision semiconductor parameter analyzer. The photocurrent and gain of APDs were measured with the help of a 1550 nm laser with an incident power of 2 mW. For the gain calculation, the difference between the total currents with and without illumination at a particular bias was normalized with the unity-gain photocurrent. The difference between the total currents at zero bias was used as the reference for unity-gain photocurrent.

3. Results and discussion

The electrical performance was examined by obtaining the diode characteristics in the voltage range from -1.0 V to 1.0 V at 77 K. As shown in Fig. 2, both $p^+n^-n^+$ and $p^+nn^-n^+$ devices have exhibited a low dark current density, which is 1.5×10^{-7} A/cm^2 and 1.8×10^{-8} A/cm^2 at -0.1 V, respectively. Furthermore, although the dark current density of the $p^+nn^-n^+$ device is nearly one order of magnitude lower than that of the $p^+n^-n^+$ device from 0 to -1.0 V, its dark current density increases dramatically in the voltage range from 0 V to -0.1 V. Fortunately, for reverse bias range from -0.1 V to -1.0 V, the dark current density of the $p^+n^-n^+$ and $p^+nn^-n^+$ devices shows a slight dependency on the applied reverse bias. It is worth noting that in positive bias condition the dark current curvilinear shape of the $p^+n^-n^+$ device is relative ideal. However, the $p^+nn^-n^+$ device exhibits a turn-on characteristic, which is possibly related to the poor Ohmic contact during processing.

Figure 3 shows the spectral response and the corresponding quantum efficiency of the two devices measured by Nicolet IS50 FTIR system, calibrated by a 1000 K blackbody source with single pass configuration. It is clear that the two devices exhibit a same 100% cut-off wavelength of 2.25 μm at 77 K. Although 50% cut-off wavelength cannot be determined precisely, we estimate 50% cut-off wavelength of the two samples to be around 2.03 μm. The cut-off wavelength is measured to be shorter than the design of 2 ML/8 ML presumably due to growth variation or relatively thin absorber layer. At a reverse bias of -0.1 V at 77 K, the $p^+n^-n^+$ and $p^+nn^-n^+$ devices demonstrate a peak responsivity about 0.35 A/W and

0.40 A/W at 1.5 μm, corresponding to a quantum efficiency of 29% and 32.4%, respectively. The peak specific detectivities are then calculated to be 1.58×10^{12} cm·Hz$^{1/2}$/W and 4.9×10^{12} cm·Hz$^{1/2}$/W at 1.5 μm, respectively.

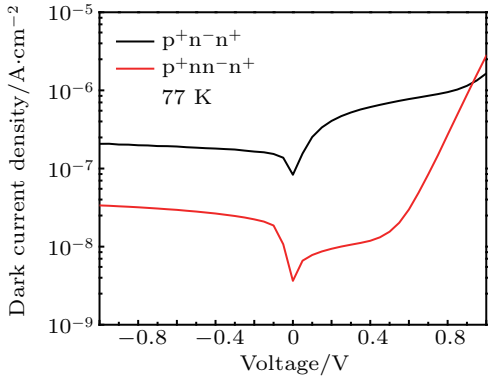


Fig. 2. The dark current density as a function of applied bias for the p$^+$n$^-$n$^+$ and p$^+$nn$^-$n$^+$ devices measured under 77 K.

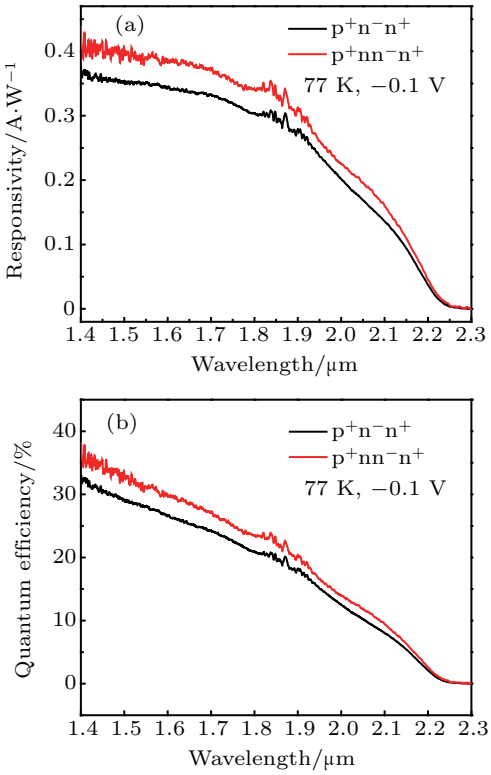


Fig. 3. The comparison of (a) spectral responsivity and (b) quantum efficiency for p$^+$n$^-$n$^+$ and p$^+$nn$^-$n$^+$ devices.

Figure 4 shows the typical breakdown and gain characteristics of the h-APDs. For the p$^+$n$^-$n$^+$ device in Fig. 4(a), a maximum multiplication gain of less than 2 was achieved at a reverse bias of −15 V at 77 K. In contrast, an improved gain characteristic was observed in the p$^+$nn$^-$n$^+$ device. In Fig. 4(b), a maximum multiplication gain about 55 was achieved at a reverse bias of −15 V at 77 K. The multiplication gain of the p$^+$nn$^-$n$^+$ device is much higher than that of the p$^+$n$^-$n$^+$ device, which can be attributed to the higher electric field in the p$^+$nn$^-$n$^+$ device. However, it also leads to an earlier tunneling and a higher dark current at a bias voltage higher than −4 V, and thus degraded device performance, as shown in Fig. 4(b). As a result, the excess noise factor could not be measured due to the high current. Nevertheless, the exponential nature of the gain characteristic indicates a single carrier dominated avalanche mechanism as reported by other works.[13–15] It is obviously that the p$^+$nn$^-$n$^+$ device has attained exponential multiplication gain behavior and demonstrated the single carrier dominated h-APDs operation.

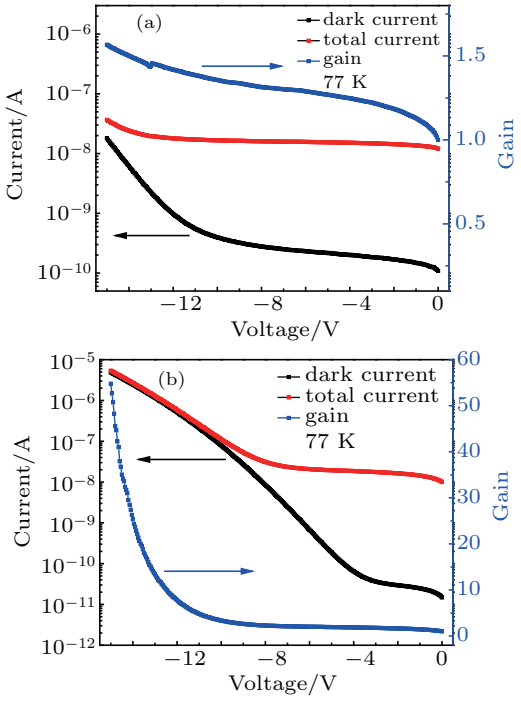


Fig. 4. Total current with illumination, dark current, and corresponding multiplication gain vs. applied reverse bias for the (a) p$^+$n$^-$n$^+$ device, and (b) p$^+$nn$^-$n$^+$ device at 77 K.

As mentioned above, two homojunction SWIR h-APDs have been designed and fabricated. Although the p$^+$nn$^-$n$^+$ device has realized a high multiplication gain performance, it still faces the detrimental effect of increasing tunneling current. To solve this problem, a heterojunction design with a wider-bandgap multiplication layer will be helpful to lower the tunneling current. Further work is currently going on to explore the effectiveness of the heterojunction design in InAs/GaSb SLs h-APDs.

4. Conclusion

We have demonstrated two homojunction SWIR h-APDs based on InAs/GaSb SLs grown by MOCVD on InAs substrate. Comparing with the baseline p$^+$n$^-$n$^+$ device, the p$^+$nn$^-$n$^+$ device with elaborate and precise electric field distribution control showed an improved device performance. At a reverse bias of −0.1 V at 77 K, the 100% cut-off wavelength and 50% cut-off wavelength were 2.25 μm and 2.03 μm for both devices, respectively. The p$^+$n$^-$n$^+$ and p$^+$nn$^-$n$^+$ devices showed a dark current density as low as 1.5×10^{-7} A/cm^2

and 1.8×10^{-8} A/cm^2, and a specific detectivity of 1.58×10^{12} cm·Hz$^{1/2}$/W and 4.9×10^{12} cm·Hz$^{1/2}$/W, respectively. Moreover, the $p^+nn^-n^+$ device exhibited a maximum multiplication gain of 55 while the $p^+n^-n^+$ device attained a maximum multiplication gain of less than 2. These results have demonstrated the feasibility of InAs/GaSb SLs SWIR h-APDs grown by MOCVD. Further improvement of device performance can be expected by adopting a heterojunction structure and suppressing the tunneling current.

References

[1] Nguyen B M, Chen G X, Hoang M A and Razeghi M 2011 *IEEE J. Quantum. Elect.* **47** 686

[2] Smith D L and Mailhiot C 1987 *J. Appl. Phys.* **62** 2545

[3] Rogalski A and Martyniuk P 2006 *Infrared. Phys. Techn.* **48** 39

[4] Banerjee K, Mallick S, Ghosh S, Plis E, Rodriguez J B, Krishna S and Grein C 2008 *Mater. Res. Soc. Proc.* **1076** 1076-K02

[5] Mallick S, Banerjee K, Ghosh S, Plis E, Rodriguez J B, Krishna S and Grein C 2007 *Appl. Phys. Lett.* **91** 241111

[6] Banerjee K, Ghosh S, Mallick S, Plis E, Krishna S and Grein C 2009 *Appl. Phys. Lett.* **94** 201107

[7] Nishida K, Taguchi K and Matsumoto Y 1979 *Appl. Phys. Lett.* **35** 251

[8] David J P R and Tan C H 2008 *IEEE J. Sel. Top. Quantum Electron.* **14** 998

[9] Hoffman D, Nguyen B M, Delaunay P Y, Hood A, Razeghi M and Pellegrino J 2007 *Appl. Phys. Lett.* **91** 143507

[10] Yang Q K, Fuchs F, Schmitz J and Pletschen W 2002 *Appl. Phys. Lett.* **81** 4757

[11] Li X, Zhao Y, Wu Q H, Teng Y, Hao X J and Huang Y 2018 *J. Cryst. Growth.* **502** 71

[12] Chen Y, Liu J F, Zhao Y, Teng Y, Hao X J, Li X, Zhu H, Zhu H, Wu Q H and Huang Y 2020 *Infrared. Phys. Techn.* **105** 103209

[13] Kinch M A, Beck J D, Wan C F, Ma F and Campbell J 2004 *J. Electron. Mater.* **33** 630

[14] Beck J, Wan C, Kinch M, Robinson J, Mitra P, Scritchfield R, Ma F and Campbell J 2006 *J. Electron. Mater.* **35** 1166

[15] Ghosh S, Mallick S, Banerjee K, Grein C, Velicu S, Zhao J, Silversmith D, Rodriguez J B, Plis E and Krishna S 2008 *J. Electron. Mater.* **37** 1764